Modeling Micro Mass and Heat Transfer for Gases Using Extended Continuum Equations

Manuel Torrilhon
Seminar for Applied Mathematics,
ETH Zurich,
Zurich 8092, Switzerland
e-mail: matorril@math.ethz.ch

Henning Struchtrup
Department of Mechanical Engineering,
University of Victoria,
PO Box 3055 STN CSC,
Victoria BC V8W 3P6, Canada
e-mail: struchtr@uvic.ca

This paper presents recent contributions to the development of macroscopic continuum transport equations for micro gas flows and heat transfers. Within the kinetic theory of gases, a combination of the Chapman–Enskog expansion and the Grad moment method yields the regularized 13-moment equations (R13 equations), which are of high approximation order. In addition, a complete set of boundary conditions can be derived from the boundary conditions of the Boltzmann equation. The R13 equations are linearly stable, and their results for moderate Knudsen numbers stand in excellent agreement with direct simulation Monte Carlo (DSMC) method simulations. We give analytical expressions for heat and mass transfer in microchannels. These expressions help to understand the complex interaction of fluid variables in microscale systems. Additionally, we compare interesting analogies such as a mass flux and energy Knudsen paradox. In particular, the R13 model is capable of predicting and explaining the detailed features of Poiseuille microflows. [DOI: 10.1115/1.3056598]

Keywords: continuum models, Poiseuille flow, moment method, kinetic gas theory

1 Introduction

Processes in microscale flows of gases or, equivalently, in rarefaction situations are well described by the Boltzmann equation [1], which describes the evolution of the particle distribution function in phase space, i.e., on the microscopic level.

The relevant scaling parameter to characterize processes in microflow gases is the Knudsen number Kn, defined as the ratio between the mean free path of a particle and a relevant length scale. If the Knudsen number is small, the Boltzmann equation can be reduced to simpler models, which allow faster solutions. Indeed, if the Knudsen number is small ($\mathrm{Kn} < 0.01$), the hydrodynamic equations, the laws of Navier–Stokes and Fourier (NSF), can be derived from the Boltzmann equation, e.g., by the Chapman-Enskog method [2]. The NSF equations are macroscopic equations for mass density ρ, velocity v_i, and temperature T and thus pose a mathematically less complex problem than the Boltzmann equation.

Macroscopic equations for rarefied gas flows at Knudsen numbers above 0.01 promise to replace the Boltzmann equation with simpler equations that still capture the relevant physics. The Chapman–Enskog expansion is the classical method to achieve this goal, but the resulting Burnett and super-Burnett equations are unstable [3]. To fix these problems in the framework of the Chapman–Enskog expansion is cumbersome [4,5]. Nevertheless, in some cases Burnett equations could be used for simulations of nonequilibrium gases [6–8].

A classical alternative is Grad's moment method [9], which extends the set of variables by adding deviatoric pressure tensor $\sigma_{ij} := p_{\langle ij \rangle}$ (stress), heat flux q_i, and possibly higher moments of the velocity distribution function (phase density) of the particles. The resulting equations are stable but lead to spurious discontinuities in shocks [10]. Nevertheless, some successes have been obtained with moment methods, and popularity is rising (see Refs. [11–15]). However, for a given value of the Knudsen number, it is not clear what set of moments one would have to consider [2].

Struchtrup and Torrilhon [16,17] combined both approaches by performing a Chapman–Enskog expansion around a nonequilibrium phase density of Grad type, which resulted in the "regularized 13-moment equations" (R13 equations), which form a stable set of equations for the 13 variables $(\rho, v_i, T, \sigma_{ij}, q_i)$ of super-Burnett order, i.e., of third order in the Knudsen number when asymptotically expanded. Section 2 gives a review of this original derivation. An alternative approach to the problem was presented by Struchtrup in Refs. [18,19], partly based on an earlier work by Müller et al. [20]. This order-of-magnitude method is based on a rigorous asymptotic analysis of the infinite hierarchy of the moment equations. A brief outline is also given in Sec. 2.

One of the biggest problems for all models beyond NSF is to prescribe suitable boundary conditions for the extended equations, which should follow from the boundary conditions for the Boltzmann equation. This task was recently tackled in Ref. [21], and the general solution to the problem [22] will be discussed after the derivation of the equations when we present boundary conditions for the R13 equations.

The second part of this paper will survey the properties of the R13 equations, which are linearly stable, obey an H-theorem for the linear case, contain the Burnett and super-Burnett equations asymptotically, predict phase speeds and damping of ultrasound waves in excellent agreement with experiments, yield smooth and accurate shock structures for all Mach numbers, and exhibit Knudsen boundary layers and the Knudsen minimum of channel flow in excellent agreement with direct simulation Monte Carlo (DSMC) method simulations. This paper reviews detailed information about the performance of R13 for Poiseuille flow in microchannels and discusses how microvariables enter and influence the classical fluid dynamical relations. The interested reader is referred to the cited literature, including the monograph [2].

2 Derivation of R13

The derivation of the regularized 13-moment equations has been done in two ways. Both ways give specific insight into the structure and properties of the theory.

2.1 Based on Pseudo-Time-Scales. The original derivation

Contributed by the Heat Transfer Division ASME for publication in the JOURNAL OF HEAT TRANSFER. Manuscript received February 10, 2008; final manuscript received August 16, 2008; published online January 13, 2009. Review conducted by Robert D. Tzou. Paper presented at the 2008 International Conference on Micro/Nanoscale Heat Transfer (MNHT2008), January 6–9 2008, Tainan, Taiwan.

[16] develops an enhanced constitutive theory for Grad's moment equations. The closure procedure of Grad is too rigid and needs to be relaxed. The new theory can be summarized in three steps:

1. Identify the set of variables U and higher moments V that need a constitutive relation in Grad's theory.
2. Formulate evolution equations for the difference $R=V-V^{(\mathrm{Grad})}(U)$ of the constitutive moments and their Grad relation.
3. Perform an asymptotic expansion of R alone while fixing *all* variables U of Grad's theory.

This procedure can, in principle, be performed on any system obtained by Grad's moment method; i.e., any number of moments can be considered as a basic set of variables. For the derivation of R13 the first 13-moment density, velocity, temperature, stress deviator, and heat flux have been considered in accordance with the classical 13-moment case of Grad.

In the classical Grad approach, the difference R is considered to be zero: All constitutive moments follow from lower moments by means of Grad's distribution $V=V^{(\mathrm{Grad})}(U)$. This rigidity causes hyperbolicity as well as artifacts such as subshocks and poor accuracy. However, the evolution equation for R is, in general, not an identity. Instead it describes possible deviations of Grad's closure. The constitutive theory of R13 takes these deviations into account.

The evolution equation for R cannot be solved exactly because it is influenced by even higher moments. Hence, an approximation is found by asymptotic expansion. In doing this, step 3 requires a modeling assumption about a scaling cascade of the higher order moments. In the asymptotic expansion of R, we fix lower moments, that is, density, velocity, and temperature, as well as nonequilibrium quantities such as stress and heat flux. The assumption is a pseudo-time-scale such that the higher moments R follow a faster relaxation. The expansion can also be considered as an expansion around a nonequilibrium (pseudo-equilibrium). A similar idea has been formulated in Ref. [23] based solely on distribution functions.

The result for R after one expansion step is a relation that couples R to gradients of the variables U; in R13 these are gradients of stress and heat flux. The gradient terms enter the divergences in the equations for stress and heat flux and produce dissipative second order derivatives. The final system is a regularization of Grad's 13-moment equations. The procedure resembles the derivation of the NSF system. Indeed the NSF equations can be considered as a regularization of Euler equations (i.e., Grad's five-moment system).

2.2 Based on Order of Magnitude. The order-of-magnitude method [18,19] considers the infinite system of moment equations resulting from Boltzmann's equation. It does not depend on Grad's closure relations and does not directly utilize the result of asymptotic expansions. The method finds the proper equations with the order of accuracy λ_0 in the Knudsen number by the following three steps:

1. determination of the order of magnitude λ of the moments
2. construction of moment set with a minimum number of moments at order λ
3. deletion of all terms in all equations that would lead only to contributions of orders $\lambda>\lambda_0$ in the conservation laws for energy and momentum

Step 1 is based on a Chapman–Enskog expansion where a moment φ is expanded according to $\varphi=\varphi_0+\mathrm{Kn}\varphi_1+\mathrm{Kn}^2\varphi_2+\cdots$, and the leading order of φ is determined by inserting this ansatz into the complete set of moment equations. A moment is said to be of leading order λ if $\varphi_\beta=0$ for all $\beta<\lambda$. This first step agrees with the ideas of Ref. [20]. Alternatively, the order of magnitude of the moments can be found from the principle that a single term in an equation cannot be larger in size by one or several orders of magnitude than all other terms [24].

In step 2, new variables are introduced by a linear combination of the moments originally chosen. The new variables are constructed such that the number of moments at a given order λ is minimal. This step gives an unambiguous set of moments at order λ.

Step 3 follows from the definition of the order of accuracy λ_0: A set of equations is said to be accurate of order λ_0 when stress and heat flux are known within the order $\mathcal{O}(\mathrm{Kn}^{\lambda_0})$.

The order-of-magnitude method gives the Euler and NSF equations at zeroth and first orders and thus agrees with the Chapman–Enskog method in the lower orders [18]. The second order equations turn out to be Grad's 13-moment equations for Maxwell molecules [18] and a generalization of these for molecules that interact with power potentials [2,19]. At third order, the method was only performed for Maxwell molecules, where it yields the R13 equations [18]. It follows that R13 satisfies some optimality when processes are to be described with third order accuracy.

Note that the derivation based on pseudo-time-scales above requires an unphysical assumption, namely, strongly different relaxation times for different moments. Such a cascading does not exist since all moments relax on roughly the same time scale proportional to Kn. The order-of-magnitude approach does not rely on such an assumption. Instead of different relaxation times, this method induces a structure on the set of nonequilibrium moments based on size, that is, order of magnitude, and justifies different closed systems of moment equations.

2.3 Result. Here, we display the original R13 equations from Ref. [16], which are build from the general conservation laws for a monatomic gas with mass density ρ, velocity v_i, and temperature θ in energy units,

$$\frac{\partial \varrho}{\partial t}+\frac{\partial \varrho v_k}{\partial x_k}=0 \tag{1}$$

$$\varrho\frac{\partial v_i}{\partial t}+\varrho v_k\frac{\partial v_i}{\partial x_k}+\frac{\partial p}{\partial x_i}+\frac{\partial \sigma_{ik}}{\partial x_k}=0 \tag{2}$$

$$\frac{3}{2}\varrho\frac{\partial \theta}{\partial t}+\frac{3}{2}\varrho v_k\frac{\partial \theta}{\partial x_k}+\frac{\partial q_k}{\partial x_k}+(p\delta_{ij}+\sigma_{ij})\frac{\partial v_i}{\partial x_j}=0 \tag{3}$$

where δ_{ij} is the Kronecker symbol or identity matrix. For the pressure p we assume the ideal gas law $p=\rho\theta$. We use Cartesian index notation with $i,j,k,l\in\{1,2,3\}$ and summation convention. The additional evolution equations that close the system are given by

$$\frac{\partial \sigma_{ij}}{\partial t}+\frac{\partial \sigma_{ij}v_k}{\partial x_k}+\frac{4}{5}\frac{\partial q_{\langle i}}{\partial x_{j\rangle}}+2p\frac{\partial v_{\langle i}}{\partial x_{j\rangle}}+2\sigma_{k\langle i}\frac{\partial v_{j\rangle}}{\partial x_k}+\frac{\partial m_{ijk}}{\partial x_k}=-\frac{p}{\mu}\sigma_{ij} \tag{4}$$

for the stress deviator σ_{ij} and

$$\frac{\partial q_i}{\partial t}+\frac{\partial q_i v_k}{\partial x_k}+p\frac{\partial(\sigma_{ik}/\rho)}{\partial x_k}+\frac{5}{2}(p\delta_{ik}+\sigma_{ik})\frac{\partial \theta}{\partial x_k}-\frac{\sigma_{ij}}{\varrho}\frac{\partial \sigma_{jk}}{\partial x_k}+\left(m_{ijk}+\frac{6}{5}q_{(i}\delta_{jk)}+q_k\delta_{ij}\right)\frac{\partial v_j}{\partial x_k}+\frac{1}{2}\frac{\partial \hat{R}_{ik}}{\partial x_k}=-\frac{2p}{3\mu}q_i \tag{5}$$

for the heat flux q_i with μ the viscosity of the gas. Round brackets give the symmetric part of a tensor, while angular brackets around indices denote the symmetric deviatoric part, e.g., $A_{\langle ij\rangle}=A_{(ij)}-\frac{1}{3}A_{kk}\delta_{ij}=\frac{1}{2}(A_{ij}+A_{ji})-\frac{1}{3}A_{kk}\delta_{ij}$, and analogously for three indices, see Ref. [2].

Note that these equations include the classical laws of Navier–Stokes and Fourier for stress deviator and heat flux. They can be

formally recovered by setting σ_{ij}, q_i, m_{ijk}, and $\hat{R}_{ij}$ to zero on the left hand side only. The additional terms in the equations beyond the classical laws allow for inertial effects and nongradient transport. That is, stress and heat flux are no longer slaved to the thermodynamic fluxes, velocity gradient, and temperature gradient.

The remaining quantities m_{ijk} and $\hat{R}_{ij}$ represent higher moments, and as such they form fluxes of stress and heat flux. These are zero in the Grad case, but the R13 theory provides the gradient expressions

$$m_{ijk} = -2\mu \frac{\partial(\sigma_{\langle ij}/\rho)}{\partial x_{k\rangle}} + \frac{8}{10p} q_{\langle i} \sigma_{jk\rangle}^{(\mathrm{NSF})} \tag{6}$$

$$R_{ij} = -\frac{24}{5}\mu \frac{\partial(q_{\langle j}/\rho)}{\partial x_{j\rangle}} + \frac{32}{25p} q_{\langle i} q_{j\rangle}^{(\mathrm{NSF})} + \frac{24}{7\rho} \sigma_{k\langle i} \sigma_{j\rangle k}^{(\mathrm{NSF})} \tag{7}$$

$$R = -12\mu \frac{\partial(q_k/\rho)}{\partial x_k} + \frac{8}{p} q_k q_k^{(\mathrm{NSF})} + \frac{6}{\rho} \sigma_{ij} \sigma_{ij}^{(\mathrm{NSF})} \tag{8}$$

with $\hat{R}_{ij} = R_{ij} + \frac{1}{3} R \delta_{ij}$ and the abbreviations

$$\sigma_{ij}^{(\mathrm{NSF})} = -2\mu \frac{\partial v_{\langle i}}{\partial x_{j\rangle}}, \quad q_i^{(\mathrm{NSF})} = -\frac{15}{4}\mu \frac{\partial \theta}{\partial x_i} \tag{9}$$

In total the R13 system is given by nonlinear parabolic-hyperbolic partial differential equations with relaxation. In that sense it resembles the mathematical structure of the NSF equations.

3 Boundary Conditions for R13

The computation of boundary conditions for the R13 equations is based on Maxwell's model for boundary conditions for the Boltzmann equation [1,2,25], which states that a fraction χ of the particles hitting the wall are thermalized, while the remaining $1-\chi$ particles are specularly reflected. Boundary conditions for moments follow by taking moments of the boundary conditions of the Boltzmann equation. To produce meaningful boundary conditions, one needs to obey the following rules:

1. *Continuity*: In order to have meaningful boundary conditions for all accommodation coefficients $\chi \in [0,1]$, only boundary conditions for tensors with an odd number of normal components should be considered [21].
2. *Consistency*: Only boundary conditions for fluxes that actually appear in the equations should be considered [22].
3. *Coherence*: The same number of boundary conditions should be prescribed for the linearized and the nonlinear equations [22].

The application of rules 1 and 2 is straightforward and yields the following set of kinetic boundary conditions (t and n denote tangential and normal tensor components, respectively) for moments:

$$\begin{aligned}
\sigma_{tn} &= -\beta\left(PV_t + \tfrac{1}{2} m_{tnn} + \tfrac{1}{5} q_t\right) \\
q_n &= -\beta\left(2P\Delta\theta + \tfrac{5}{28} R_{nn} + \tfrac{1}{15} R + \tfrac{1}{2}\theta\sigma_{nn} - \tfrac{1}{2} PV_t^2\right) \\
R_{tn} &= \beta\left(P\theta V_t - \tfrac{1}{2}\theta m_{tnn} - \tfrac{11}{5}\theta q_t - PV_t^3 + 6P\Delta\theta V_t\right) \\
m_{nnn} &= \beta\left(\tfrac{2}{5} P\Delta\theta - \tfrac{1}{14} R_{nn} + \tfrac{1}{75} R - \tfrac{7}{5}\theta\sigma_{nn} - \tfrac{3}{5} PV_t^2\right) \\
m_{ttn} &= -\frac{m_{nnn}}{2} - \beta\left(\frac{1}{14}\left(R_{tt} + \frac{R_{nn}}{2}\right) + \theta\left(\sigma_{tt} + \frac{\sigma_{nn}}{2}\right) - PV_t^2\right)
\end{aligned} \tag{10}$$

where $\Delta\theta = \theta - \theta_W$, $V_t = v_t - v_t^W$, and

$$P := \rho\theta + \frac{\sigma_{nn}}{2} - \frac{R_{nn}}{28\theta} - \frac{R}{120\theta} \tag{11}$$

The properties of the wall are given by its temperature θ_W and velocity v_t^W and the modified accommodation coefficient

$$\beta = \chi/(2-\chi)\sqrt{2/(\pi\theta)} \tag{12}$$

In extrapolation of the theory of accommodation, these coefficients that occur in every equation of Eq. (10) could be chosen differently. So far, most results have been obtained with only one accommodation coefficient in accordance with the Maxwell model. Clearly, the Maxwell model is a strong reduction of the wall properties, and in many realistic cases more parameters are required to model wall interactions. Different accommodation coefficients of the single moment fluxes, e.g., shear or heat flux, could be used to model detailed wall properties. However, more investigations and comparisons are required for such an approach.

The first condition above is the slip condition for the velocity, while the second equation is the jump condition for the temperature. They come in a generalized form, with the essential part given by $\sigma_{tn} \sim V_t$ and $q_n \sim \Delta\theta$. In a manner of speaking, the other conditions can be described as jump conditions for higher moments, which again relate fluxes and respective variables. In perfect analogy to the usual slip and jump conditions, the essential part is given by $R_{tn} \sim q_t$ and $m_{nnn} \sim \sigma_{nn}$. The additional terms in Eq. (10) are off-diagonal terms coupling all even (in index n) moments in the boundary conditions.

When the R13 equations are considered for channel flows in their original form, it turns out that a different number of boundary conditions is required to solve the fully nonlinear and the linearized equations. Since this would not allow a smooth transition between linear and nonlinear situations, we formulated the third rule as given above.

Asymptotic analysis shows that some terms can be changed without changing the overall asymptotic accuracy of the R13 equations. This leads to the algebraization of several nonlinear terms in the partial differential equations, which, after some algebra, leads to algebraic relations, termed as bulk equations, between the moments that serve as additional boundary conditions for the nonlinear equations [22],

$$m_{tnn} = \frac{32}{45p} \sigma_{tn} q_n \tag{13}$$

$$\hat{R}_{nn} = \frac{136}{25p} q_n^2 - \frac{72}{35\rho} \sigma_{tn}^2 \tag{14}$$

These equations have a special interpretation. The possibility to prescribe kinetic boundary conditions as in Eq. (10) for moments is related to the ability of the moments to produce a so-called Knudsen layer. The Knudsen layer is a boundary layer that occurs close to the wall in high Knudsen number flows, for example, in microchannels. The kinetic boundary condition specifies the amplitude of the boundary layer. In the R13 system some variables, for instance, parallel heat flux, and normal stresses, are able to produce a Knudsen layer, while the higher moments $\hat{R}_{nn}$ and m_{tnn} cannot. This is due to the finite number of moments considered. In the infinite moment hierarchy, all moments exhibit Knudsen layers (see Ref. [26]).

Due to the lack of a Knudsen layer, kinetic boundary conditions may not be used for the moments $\hat{R}_{nn}$ and m_{tnn}. Instead, we assume that the boundary layer is relaxed infinitely fast to an interior solution—the bulk relation given in Eq. (13). The analysis shows that relation (13) is valid not only at the boundary but also at some distance from it where the flow has shear flow character. In that sense the bulk relations are consistency requirements and not only boundary conditions. They are algebraic relations required by the R13 equations, and the values for $\hat{R}_{nn}$ and m_{tnn} at the wall need to be consistent. Correspondingly, Eq. (13) should be

prescribed at the wall. Hence, the bulk solution turns out to be the natural boundary conditions for Knudsen-layer-less variables. Details of this interpretation can be found in Ref. [22].

4 Achievements With R13

We summarize the most important features of the R13 equations, which result from analytical considerations and from analytical and numerical solutions. The results of R13 have been compared with experimental data as well as to direct simulation results obtained by DSMC [27].

The R13 equations

- are derived in a rational manner by means of the order-of-magnitude method [18,19] or from a Chapman–Enskog expansion around nonequilibrium [16,17], as described above
- are of third order in the Knudsen number [2,16–19] when expanded in an asymptotic expansion and compared with the full expansion of Boltzmann's equation
- are linearly stable for initial and boundary value problems [16,17] (that is, amplitudes of linear sound and heat waves are not amplified)
- contain Burnett and super-Burnett asymptotically in the linear [16] and nonlinear [17] cases (however, higher order contributions stabilize the R13 system)
- predict phase speeds and damping of sound waves with high frequencies and short wavelengths in excellent agreement with experiments [16]
- give smooth shock structures without subshocks for all Mach numbers, with quantitatively very good agreement with DSMC simulations for $\mathrm{Ma} \lesssim 3$ [17]
- are accompanied by a complete set of boundary conditions [22] based on the most commonly used accommodation model in kinetic theory
- obey an entropy and H-theorem for the linear case, including the boundaries [28], which can also be used to derive the equations as such
- exhibit the Knudsen paradox, i.e., the minimum of the mass flow rate for channel flows (see Sec. 5) [22,28]
- exhibit Knudsen boundary layers for temperature and velocity profiles as well as other moments in good agreement with DSMC [29,30]
- are easily accessible to numerical simulations in multiple space dimensions based on finite volume methods [31] or pressure-correction schemes [21]
- predict dynamic form factors [32] in accordance with experiments of light scattering spectra measuring small scale density fluctuations

We proceed with presenting the details of microchannel flows.

5 Microchannel Flows

To approach microchannel flows, we study a special class of steady shear flows that include steady Couette or Poiseuille flows. For the R13 system, shear flow is a multidimensional phenomenon in the sense that it produces a fully multidimensional reaction for the stress tensor and heat flux. Introducing $x_i \hat{=} (x,y,z)$, we consider shear flow, which is homogeneous in the z-direction, and define the remaining nonvanishing parts of stress tensor and heat flux as

$$\sigma = \begin{pmatrix} \sigma_{xx} & \sigma_{xy} & 0 \\ \sigma_{yx} & \sigma_{yy} & 0 \\ 0 & 0 & \sigma_{zz} \end{pmatrix}, \quad \mathbf{q} = (q_x, q_y, 0) \tag{15}$$

where $\sigma_{xy} = \sigma_{yx}$ and $\sigma_{zz} = -(\sigma_{xx} + \sigma_{yy})$ since σ must be trace free. For the velocity we assume $v_y = v_z = 0$ and

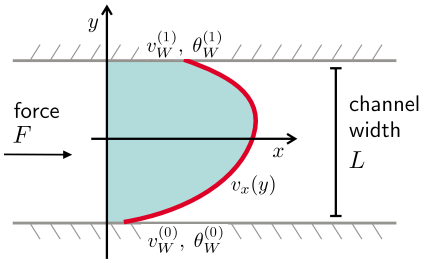

Fig. 1 General setting for shear flow between two infinite plates. The plates are moving and may be heated.

$$\mathbf{v}(x,y,z) = (v_x(y), 0, 0) \tag{16}$$

The force acts only in the x-direction, $\mathbf{f} = (F,0,0)$ and enters the momentum balance (2) but no other equation. This setting is valid for channel flows, as displayed in Fig. 1. The gas is confined between two infinite plates at distance L and moves solely in the x-direction. The walls are moving with x-velocities $v_W^{(0,1)}$ and may be heated with different temperatures $\theta_W^{(0,1)}$. The Knudsen number $\mathrm{Kn} = \lambda / L$ with mean free path $\lambda = \mu / (\rho \sqrt{\theta})$ is based on the width of the channel.

In this setting we have eight independent variables in the R13 equations, namely, $\{\rho, v_x, p, \sigma_{xx}, \sigma_{yy}, \sigma_{xy}, q_x, q_y\}$. Optionally, the pressure p can be replaced by the temperature θ. The five remaining relevant constitutive quantities are $\{m_{xxy}, m_{xyy}, m_{yyy}, \hat{R}_{xy}, \hat{R}_{yy}\}$. Systems (1)–(9) reduces to 13 first order nonlinear ordinary differential equations in the space variable y. The equations uncover a striking simplicity by decomposing into three linearly decoupled blocks. The coupling is displayed by writing the vector of variables in the form

$$\mathbf{U} = \{v_x, \sigma_{xy}, q_x, m_{xyy}, R_{xy} | \theta, q_y, \sigma_{yy}, \hat{R}_{yy}, m_{yyy} | \rho, \sigma_{xx}, m_{xxy}\} \tag{17}$$

The first block describes the velocity part with the balances of v_x, σ_{xy}, and q_x and higher moments m_{xyy} and $\hat{R}_{xy}$; the second block describes the temperature part with the balances of θ, q_y, and σ_{yy} and higher moments $\hat{R}_{yy}$ and m_{yyy}. Both parts are governed dominantly by two classical variables, (v_x, σ_{xy}) and (θ, q_y), respectively, which behave essentially in an intuitive way. In NSF the second variable is related to the gradient of the first. The third variable in both parts, q_x and σ_{yy}, respectively, is given by a seemingly classical variable, which, however, plays a nonintuitive role. It represents a *heat flux produced by a velocity shear* in the first block and a *normal stress due to temperature difference* in the second. Both are typical rarefaction effects in microflows of gases. Through these variables the classical variables velocity and temperature are coupled to the high order internal quantities, m_{xyy} and $\hat{R}_{xy}$, and $\hat{R}_{yy}$ and m_{yyy}, respectively. From tensorial considerations, the first block can be identified with mixed normal/tangential variables (shear), while the second block couples the purely normal variables (temperature). The last block combines the density and purely tangential tensorial variables and exhibits only a minor influence.

5.1 Linear Equations and Knudsen Layers. One of the most important advantages of continuum models is the possibility to gain understanding in micro gas dynamics through analytical expressions. The mathematical structure of the equations provides a general insight into new physics and may teach intuition about complex processes.

Here, we demonstrate the rise of Knudsen layers and microscale variables, i.e., nongradient heat fluxes and normal stresses. Similar calculations can be found in Refs. [29,30].

5.1.1 Velocity Part. As mentioned above, the equations split into a velocity and a temperature part in the linear case. The

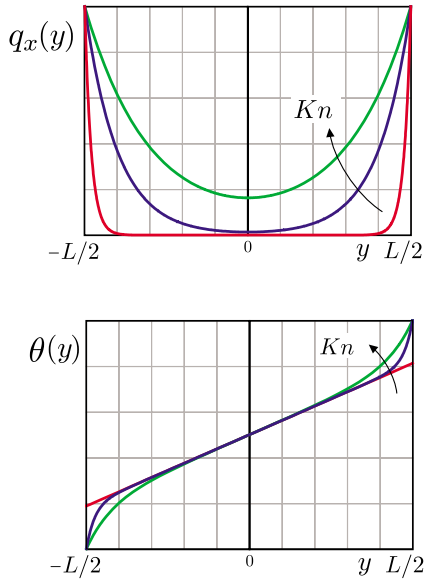

Fig. 2 R13 predicts exponential Knudsen layers for, e.g., parallel heat flux. The upper plot shows a schematic picture for *F*=0, Kn=0.01, 0.1, and 0.5. These functions lead to typical s-shaped profiles for, e.g., temperature; see the schematic lower plot with Kn=0.01, 0.1, and 0.2.

velocity part is governed by the momentum balance and an equation for shear stress, which are given by Eq. (2) with force term and the xy-component of Eq. (4) and read

$$\partial_y \sigma_{xy} = \rho F \tag{18}$$

$$\sigma_{xy} = -\mu \partial_y v_x - \frac{2}{5}\frac{\mu}{p}\partial_y q_x \tag{19}$$

with constant density, pressure, and viscosity μ. Obviously, shear stress is given by the velocity gradient and by a microscale contribution from the heat flux q_x parallel to the walls. This heat flux satisfies Eq. (5),

$$\frac{\mu}{\rho}\partial_y \sigma_{xy} + \frac{1}{2}\frac{\mu}{p}\partial_y R_{xy} = -\frac{2}{3}q_x \tag{20}$$

$$R_{xy} = -\frac{12}{5}\frac{\mu}{p}\partial_y q_x \tag{21}$$

with higher order flux R_{xy} given by Eq. (7). In particular, the parallel heat flux is independent of a temperature gradient. It is triggered from the shear stress and boundary conditions. Elimination of R_{xy} leads to a second order ordinary differential equation for q_x with solution (assuming symmetry),

$$q_x(y) = -\frac{3}{2}\mu F + C_1 \sinh\left(\frac{\sqrt{5}}{3}\frac{1}{\mathrm{Kn}}\frac{y}{L/2}\right) \tag{22}$$

using the Knudsen number[1]

$$\mathrm{Kn} = \frac{\mu\sqrt{\theta}}{pL} \tag{23}$$

The hyperbolic sine function has the shape of a boundary layer, as can be seen in Fig. 2. This boundary layer is superimposed on a bulk solution $\sim \mu F$ in q_x. Finally, the parallel heat flux enters the velocity solution (assuming symmetry)

$$v_x(y) = C_2 + \frac{\rho F}{2\mu}\left(\left(\frac{L}{2}\right)^2 - y^2\right) - \frac{2}{5p}q_x(y) \tag{24}$$

inheriting the Knudsen layer. Hence, the velocity consists of a bulk solution given by the classical parabolic profile and a layer contribution from the parallel heat flux.

Note that the boundary layers grow quickly with the Knudsen number and fill out the channel already at Kn=0.5 (see Fig. 2). At these Knudsen numbers, the bulk and layer in Eq. (24) cannot be distinguished anymore, and the solution will show a quality in its own right with no resemblance to classical solutions.

5.1.2 Temperature Part. Remarkably, the temperature part of the linear R13 equations shows identical mathematical structures. The two basic equations are now given by the energy balance (Eq. (3)) and the equation for normal heat flux q_y (Eq. (5)), which together read

$$\partial_y q_y = 0 \tag{25}$$

$$q_y = -\kappa \partial_y \theta - \frac{2}{5}\frac{\kappa}{\rho}\partial_y \sigma_{yy} \tag{26}$$

with constant density, pressure, and heat conductivity $\kappa = \frac{15}{4}\mu$ (temperature in energy units). Again, the first term on the right hand side describes Fourier's law, but the second shows the influence of normal stress σ_{yy} as a microscale variable. This normal stress is determined by Eq. (4),

$$\frac{\kappa}{p}\partial_y q_y + \frac{2}{9}\frac{\kappa}{p}\partial_y m_{yyy} = -\frac{5}{6}\sigma_{yy} \tag{27}$$

$$m_{yyy} = -\frac{8}{25}\frac{\kappa}{p}\partial_y \sigma_{yy} \tag{28}$$

with higher order flux m_{yyy} given by relation (7). Note the perfect analogy to the equations of the velocity part above. Consequently, the normal stress is given by a hyperbolic sine function (assuming antisymmetry),

$$\sigma_{yy}(y) = C_3 \sinh\left(\sqrt{\frac{5}{6}}\frac{1}{\mathrm{Kn}}\frac{y}{L/2}\right) \tag{29}$$

exhibiting boundary layer character again with the Knudsen number as the scaling parameter. This boundary layer enters the profile of the temperature,

$$\theta(y) = C_4 + \frac{C_5}{\kappa}\frac{y}{L/2} - \frac{2}{5p}\sigma_{yy}(y) \tag{30}$$

and leads to a typical s-shape, as seen in Fig. 2. The bulk solution of σ_{yy} is zero, while the bulk solution of the temperature is the classical linear function.

The integration constants C_i have to be fixed by boundary conditions, as given in Eq. (10). Similar to the equations, the boundary conditions also decouple into a velocity and a temperature part when linearized.

5.2 Mass Flux Knudsen Paradox. Gas flow through a channel is known to exhibit a paradoxical behavior known as the Knudsen paradox [33]. When reducing the Knudsen number in the experiment, the normalized mass flow rate

$$J = \int_{-1/2}^{1/2} v(y)dy \tag{31}$$

through the channel reaches a minimum and afterward starts to increase for larger Knudsen numbers.

To model this, we consider Poiseuille flow given by acceleration-driven channel flow with walls at rest and identical

[1]This definition is most suitable for dimensionless moment equations. Other definitions differ only by factors, e.g., $\widetilde{\mathrm{Kn}}$ in Ref. [3] or [6], which is $\widetilde{\mathrm{Kn}} = (4/5)\sqrt{(8/\pi)}(\mu\sqrt{\theta}/p) \approx 1.277\ \mathrm{Kn}$, or k used in Ref. [21], which is $k = (4/5)\sqrt{2}(\mu\sqrt{\theta}/p) \approx 1.13\ \mathrm{Kn}$.

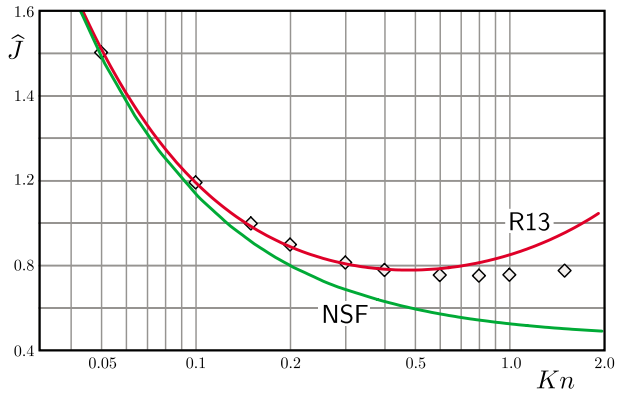

Fig. 3 Averaged mass flow rate in acceleration-driven channel flow. The R13 equations predict the Knudsen paradox.

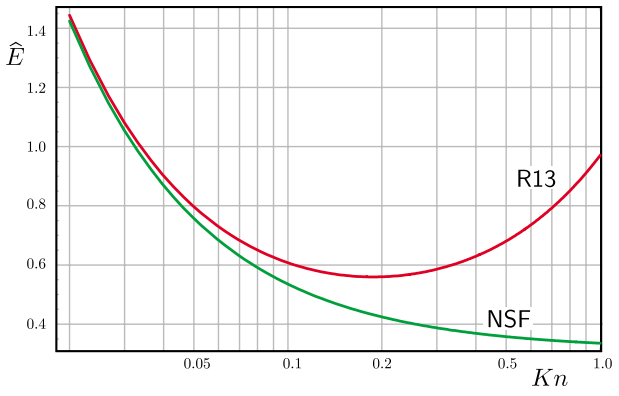

Fig. 4 R13 predicts an energy Knudsen paradox: The normalized total energy content of an externally heated channel shows a nonintuitive minimum when plotted against the Knudsen number. Standard NSF does not show this minimum.

temperatures. The channel is considered to be infinitely long such that a steady velocity profile has developed from the viscous boundary layers. The given acceleration can be interpreted as a homogeneous pressure gradient.

Given the analytical result for the channel flow of the linear R13 system above, it is easy to determine an explicit function for the mass flow rate. After integration we find

$$J = \frac{\gamma_1}{\mathrm{Kn}} + \gamma_2 \mathrm{Kn} + \gamma_3$$

where $\gamma_{1,2,3}$ depend on the coefficients in the equations and boundary conditions, essentially, viscosity and accommodation factor. The functional dependence on the Knudsen number is valuable information. In general, the coefficients could also be calibrated to measurements.

Figure 3 shows the dimensionless mass flow rate obtained from R13 as a function of Kn. The curve clearly shows a minimum and thus correctly predicts a Knudsen paradox. The figure also shows the mass flow rate obtained with NSF and standard slip boundary conditions, which clearly fails to produce a Knudsen minimum. In Ref. [34] the mass flow rate has been calculated based on the linearized Boltzmann equation, and those results are given in Fig. 3 as symbols. The mass flow for R13 follows the Boltzmann result fairly accurately until $\mathrm{Kn} \lesssim 1.0$ and then lifts off too quickly. At these high Knudsen numbers, the assumptions of the theory are not valid anymore.

The Knudsen paradox is essentially a boundary effect, as explained below. Hence, it is possible to tweak the NSF system to exhibit a Knudsen minimum as well when using second order slip (see, e.g., Ref. [35]). However, when comparing different models for second order slip with the R13 result, it turns out that the R13 curve gives a better fit to the Boltzmann result (see Ref. [36]). Additionally, the fields of flow variables temperature and heat flux in microchannel flows show a very interesting behavior correctly reproduced only by extended models beyond NSF (see Sec. 5.4).

Intuitively one would expect a decreasing mass flow for a smaller channel. The explanation for the minimum is the following: For very small Knudsen numbers, viscosity is almost vanishing, and a fully developed flow would exhibit a huge velocity profile, hence a very large mass flow rate. When viscosity is increased, this profile shrinks; however in the other extreme of large Knudsen numbers a different effect takes over. The interaction between the particles and the wall becomes so small due to lack of collisions that the particles merely accelerate and fall through the channel. Again, a fully developed flow of "accelerated freely falling" particles leads to an infinite mass flux. Between these two extrema, there must be a minimum. In summary, at a certain microscale the friction inside the gas becomes small and the growing slip velocity at the wall dominates the mass flow rate.

5.3 Energy Knudsen Paradox. We have seen above that the channel flow separates the R13 equations into two different systems of equations: one part for the velocity and shear and another part for the temperature and normal heat flux. The two parts exhibit mathematical identical structures in the linearized setting and allow us to transfer the specific behavior of shear flows to the analogous behavior of heat transfer.

This leads us to the prediction of an energy Knudsen paradox for heat transfer in the following sense. Let a resting monatomic gas between the two plates in Fig. 1 be heated by a constant volume source, e.g., radiation r. That is, the steady energy balance has the form $\partial_y q = r$. The total energy content between the plates is essentially the integral of the temperature θ

$$E = \frac{3}{2}\int_{-1/2}^{1/2} \theta(y)dy \tag{32}$$

when written in dimensionless form. When normalized with the energy input r, the energy content depends on the Knudsen number and the R13 theory predicts a paradoxical behavior when changing the width of the channel. When increasing the Knudsen number and decreasing the channel width, the energy content decreases, but only up to a certain Knudsen number. For a very small width, the total energy increases with Kn, which is nonintuitive.

Figure 4 shows the respective plot that compares the normalized total energy content $\hat{E}$, as predicted by R13 and NSF with first order jump conditions. As before, the standard NSF model without second order jump conditions does not show a minimum. R13 predicts an energy minimum, which is at smaller Knudsen numbers than the Knudsen minimum for the mass flux in Fig. 3.

To our knowledge there are no experimental or DSMC data to verify this prediction. However, it is very likely that such data would unveil an approximation quality of R13 similar to that of Fig. 3.

5.4 Full Solution for Poiseuille Flow. In the linear setting, the dissipation term in the energy balance is neglected and any velocity profile does not lead to a temperature rise. To see the temperature profile, the nonlinear equations have to be solved. Apart from arithmetic complexity, this is not a problem with the R13 model.

We solve the full nonlinear R13 system in forms (1)–(9) for a Poiseuille flow, as described above with kinetic boundary condition (10)–(14) for various Knudsen numbers. The mass flow rate is only a rough property of microflows, and the R13 result gives much more insight when considering the fields of the moments. Figures 5 and 6 display some fields obtained by R13 for Knudsen numbers Kn=0.068, 0.15, 0.4, and 1.0. The figures show the con-

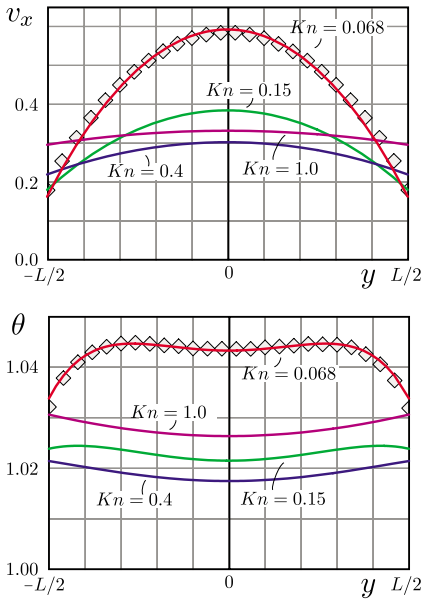

Fig. 5 Velocity and temperature profiles in acceleration-driven channel flow for various Knudsen numbers. The symbols in the case Kn=0.068 represent a DSMC result.

servation variables velocity v_x and temperature θ, as well as the microscale variables tangential heat flux q_x and normal stress σ_{yy}. Note that the channel flow produces a significant parallel heat flux q_x even though the temperature is homogeneous along x. Similarly, the temperature field triggers a normal stress even though $\partial_y v_y = 0$. This is a microscale effect. Higher Knudsen numbers show stronger nonequilibrium, as indicated by larger magnitudes of q_x and σ_{yy}. Interestingly, the temperature profile starts to invert for higher Knudsen numbers. Note also that the Knudsen paradox can be observed in the results of the R13 system in Fig. 5. The velocity profile becomes flatter, but the slip increases and the velocity curve for Kn=1.0 lies above the curve of Kn=0.4.

The simulations were obtained with a dimensionless acceleration force fixed at $F=0.23$, such that Knudsen number Kn =0.068 corresponds to the case of Poiseuille flow calculated in Ref. [37] (see also Ref. [38]) by DSMC. These results are shown in Figs. 5 and 6 as symbols. R13 gives good agreement with the DSMC result.

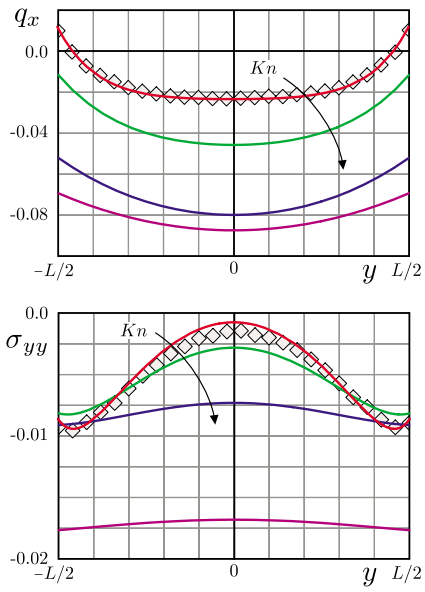

Fig. 6 Microscale effects, such as parallel heat flux q_x and normal stresses σ_{yy}, in microchannels as predicted by R13 for various Knudsen numbers. The symbols in the case Kn =0.068 represent a DSMC result.

Comparison with NSF. While the Knudsen minimum can be reproduced with the lower order system of Navier–Stokes and Fourier using higher order boundary conditions, many details of the channel flow shown above are out of scope for NSF. The temperature profile in NSF is a purely convex function with no dip and no tendency to invert for higher Knudsen numbers. NSF is also unable to predict the micro effects of parallel heat flux q_x and normal stresses σ_{yy}. Both quantities are identically zero in NSF for all Knudsen numbers because there is no temperature gradient in the x-direction and no velocity divergence.

Comparison with Ohwada et al. Ohwada et al. [34] computed Poiseuille flow results based on the linearized Boltzmann equation. They gave field curves for velocity and parallel heat flux for Kn=0.088, which are in good agreement with the R13 results and corresponding DSMC above. Especially, the parallel heat flux shows positive and negative values at this lower Knudsen number identical to the curve in 6. Unfortunately, no other fields, for example, temperature, are given in Ref. [34].

6 Conclusions and Challenges

With these properties and features, the R13 equations must be considered as the most successful continuum model for gas microflows. In contrast to direct simulations or molecular dynamics, such a model gives valuable insight into physical effects by identifying effects inside equations. The application of the R13 equations to a wider variety of microflow problems is planned for the future.

In spite of the success, the R13 equations face plenty of open challenges. From the modeling point of view, extensions to mixtures and polyatomic gases are necessary. Some ideas for such moment systems exist in the literature where internal energy variables and multiple species distribution functions are added to the kinetic description. The regularized moment approach can be applied to these settings. The current R13 equations still exhibit loss of hyperbolicity of the flux part, which leads to problems when calculating high speed flows (see Ref. [31]). The development of a globally hyperbolic flux for higher order moments is a long standing open problem. Multidimensional simulations require suitable numerical methods. Existing approaches such as those in Ref. [31] or [21] need to be refined. For slow flows as in microchannels, the hybrid numerical methods that combine classical incompressible simulation tools with compressible features caused by rarefaction effects are needed.

Interesting problems to simulate with R13 are thermal creep phenomena, for instance, in Knudsen pumps. Also, microcavity flows such as those in Refs. [39,40] are important applications.

Acknowledgment

H.S. acknowledges support by the Natural Sciences and Engineering Research Council of Canada (NSERC). M.T. acknowledges support through the EURYI award of the European Science Foundation (ESF).

References

[1] Cercignani, C., 1988, *The Boltzmann Equation and Its Applications*, Applied Mathematical Sciences Vol. 67, Springer, New York.
[2] Struchtrup, H., 2005, *Macroscopic Transport Equations for Rarefied Gas Flows*, Interaction of Mechanics and Mathematics, Springer, New York.
[3] Bobylev, A. V., 1982, "The Chapman-Enskog and Grad Methods for Solving the Boltzmann Equation," Sov. Phys. Dokl., **27**, pp. 29–31.
[4] Bobylev, A. V., 2006, "Instabilities in the Chapman-Enskog Expansion and Hyperbolic Burnett Equations," J. Stat. Phys., **124**(2–4), pp. 371–399.
[5] Jin, S., and Slemrod, M., 2001, "Regularization of the Burnett Equations Via Relaxation," J. Stat. Phys., **103**(5–6), pp. 1009–1033.
[6] Agarwal, R. K., Yun, K.-Y., and Balakrishnan, R., 2001, "Beyond Navier–

Stokes: Burnett Equations for Flows in the Continuum-Transition Regime," Phys. Fluids, **13**, pp. 3061–3085.
[7] Agarwal, R. K., Yun, K.-Y., and Balakrishnan, R., 2002, "Erratum: "Beyond Navier–Stokes: Burnett Equations for Flows in the Continuum-Transition Regime" [Phys. Fluids 13, 3061 (2001)]," Phys. Fluids, **14**, p. 1818.
[8] Lockerby, D. A., and Reese, J. M., 2003, "High-Resolution Burnett Simulations of Micro Couette Flow and Heat Transfer," J. Comput. Phys., **188**(2), pp. 333–347.
[9] Grad, H., 1949, "On the Kinetic Theory of Rarefied Gases," Commun. Pure Appl. Math., **2**, pp. 331–407.
[10] Weiss, W., 1995, "Continuous Shock Structure in Extended Thermodynamics," Phys. Rev. E, **52**, pp. R5760–R5763.
[11] Müller, I., and Ruggeri, T., 1998, *Rational Extended Thermodynamics*, Springer Tracts in Natural Philosophy Vol. 37, 2nd ed., Springer, New York.
[12] Au, J. D., Torrilhon, M., and Weiss, W., 2001, "The Shock Tube Study in Extended Thermodynamics," Phys. Fluids, **13**(8), pp. 2423–2432.
[13] Levermore, C. D., 1996, "Moment Closure Hierarchies for Kinetic Theories," J. Stat. Phys., **83**(5–6), pp. 1021–1065.
[14] Eu, B.-C., 1980, "A Modified Moment Method and Irreversible Thermodynamics," J. Chem. Phys., **73**(6), pp. 2958–2969.
[15] Myong, R.-S., 2001, "A Computational Method for Eu's Generalized Hydrodynamic Equations of Rarefied and Microscale Gas Dynamics," J. Comput. Phys., **168**(1), pp. 47–72.
[16] Struchtrup, H., and Torrilhon, M., 2003, "Regularization of Grad's 13-Moment-Equations: Derivation and Linear Analysis," Phys. Fluids, **15**(9), pp. 2668–2680.
[17] Torrilhon, M., and Struchtrup, H., 2004, "Regularized 13-Moment-Equations: Shock Structure Calculations and Comparison to Burnett Models," J. Fluid Mech., **513**, pp. 171–198.
[18] Struchtrup, H., 2004, "Stable Transport Equations for Rarefied Gases at High Orders in the Knudsen Number," Phys. Fluids, **16**(11), pp. 3921–3934.
[19] Struchtrup, H., 2005, "Derivation of 13 Moment Equations for Rarefied Gas Flow to Second Order Accuracy for Arbitrary Interaction Potentials," Multiscale Model. Simul., **3**(1), pp. 221–243.
[20] Müller, I., Reitebuch, D., and Weiss, W., 2003, "Extended Thermodynamics—Consistent in Order of Magnitude," Continuum Mech. Thermodyn., **15**(2), pp. 113–146.
[21] Gu, X., and Emerson, D., 2007, "A Computational Strategy for the Regularized 13 Moment Equations With Enhanced Wall-Boundary Conditions," J. Comput. Phys., **225**, pp. 263–283.
[22] Torrilhon, M., and Struchtrup, H., 2008, "Boundary Conditions for Regularized 13-Moment-Equations for Micro-Channels," J. Comput. Phys., **227**, pp. 1982–2011.
[23] Karlin, I. V., Gorban, A. N., Dukek, G., and Nonnenmacher, T. F., 1998, "Dynamic Correction to Moment Approximations," Phys. Rev. E, **57**(2), pp. 1668–1672.
[24] Struchtrup, H., 2006, "Scaling and Expansion of Moment Equations in Kinetic Theory," J. Stat. Phys., **125**, pp. 565–587.
[25] Maxwell, J. C., 1879, "On Stresses in Rarefied Gases Arising From Inequalities of Temperature," Philos. Trans. R. Soc. London, **170**, pp. 231–256.
[26] Struchtrup, H., 2003, "Grad's Moment Equations for Microscale Flows," AIP Conf. Proc., **663**, pp. 792–799.
[27] Bird, G. A., 1998, *Molecular Gas Dynamics and the Direct Simulation of Gas Flows*, 2nd ed., Oxford University Press, New York.
[28] Struchtrup, H., and Torrilhon, M., 2007, "H-Theorem, Regularization, and Boundary Conditions for Linearized 13 Moment Equations," Phys. Rev. Lett., **99**, p. 014502.
[29] Struchtrup, H., 2005, "Failures of the Burnett and Super-Burnett Equations in Steady State Processes," Continuum Mech. Thermodyn., **17**(1), pp. 43–50.
[30] Struchtrup, H., and Thatcher, T., 2007, "Bulk Equations and Knudsen Layers for the Regularized 13 Moment Equations," Continuum Mech. Thermodyn., **19**(3–4), pp. 177–189.
[31] Torrilhon, M., 2006, "Two-Dimensional Bulk Microflow Simulations Based on Regularized 13-Moment-Equations," Multiscale Model. Simul., **5**(3), pp. 695–728.
[32] Torrilhon, M., 2006, "Regularized 13-Moment-Equations," 25th International Symposium on Rarefied Gas Dynamics, St. Petersburg, Russia.
[33] Knudsen, M., 1909, "Die Gesetze der Molekularströmung und der inneren Reibungsströmung der Gase durch Röhren," Ann. Phys. (Leipzig), **333**, pp. 75–130.
[34] Ohwada, T., Sone, Y., and Aoki, K., 1989, "Numerical Analysis of the Poiseuille and Thermal Transpiration Flows Between Two Parallel Plates on the Basis of the Boltzmann Equation for Hard-Sphere Molecules," Phys. Fluids A, **1**(12), pp. 2042–2049.
[35] Hadjiconstantinou, N. G., 2003, "Comment on Cercignani's Second-Order Slip Coefficient," Phys. Fluids, **15**, pp. 2352–2354.
[36] Struchtrup, H., and Torrilhon, M., 2008, "Higher-Order Effects in Rarefied Channel Flows," Phys. Rev. E, **78**, p. 046301.
[37] Zheng, Y., Garcia, A. L., and Alder, J. B., 2002, "Comparison of Kinetic Theory and Hydrodynamics for Poiseuille Flow," J. Stat. Phys., **109**, pp. 495–505.
[38] Xu, K., and Li, Z.-H., 2004, "Microchannel Flow in the Slip Regime: Gas-Kinetic BGK-Burnett Solutions," J. Fluid Mech., **513**, pp. 87–110.
[39] Mizzi, S., Gu, X.-J., Emerson, D. R., Barber, R. W., and Reese, J., 2008, "Application of a High-Order Macroscopic Approach to Force-Driven Poiseuille Flow in the Slip and Transition Regimes," First International Conference on Micro- and Nano-Heat Transfer, Tainan, Taiwan, Paper No. MNHT2008-52203.
[40] Taheri, P., Torrilhon, M., and Struchtrup, H., 2008, "Couette and Poiseuille Flows in Micro-Channels: Analytical Solutions for Regularized 13-Moment Equations," in press.